

3D human interaction synthesis for action recognition data augmentation

Master Thesis



3D human interaction synthesis for action recognition data augmentation

Master Thesis

June, 2024

By

Anders Bredgaard Thuesen

Copyright: Reproduction of this publication in whole or in part must include the customary bibliographic citation, including author attribution, report title, etc.

Cover photo: Vibeke Hempler, 2012

Published by: DTU, Department of Applied Mathematics and Computer Science,
Richard Petersens Plads, Building 324, 2800 Kgs. Lyngby Denmark
www.compute.dtu.dk

ISSN: [0000-0000] (electronic version)

ISBN: [000-00-0000-000-0] (electronic version)

ISSN: [0000-0000] (printed version)

ISBN: [000-00-0000-000-0] (printed version)

Approval

This thesis has been prepared over six months at the Section for Indoor Climate, Department of Civil Engineering, at the Technical University of Denmark, DTU, in partial fulfilment for the degree Master of Science in Engineering, MSc Eng.

It is assumed that the reader has a basic knowledge in the areas of statistics.

Anders Bredgaard Thuesen - s183926

.....
Signature

.....
Date

Abstract

Hello, here is some text without a meaning. This text should show what a printed text will look like at this place. If you read this text, you will get no information. Really? Is there no information? Is there a difference between this text and some nonsense like “Huardest gefburn”? Kjift – not at all! A blind text like this gives you information about the selected font, how the letters are written and an impression of the look. This text should contain all letters of the alphabet and it should be written in of the original language. There is no need for special content, but the length of words should match the language.

Acknowledgements

Anders Bredgaard Thuesen, MSc Civil Engineering, DTU

I would like to thank my supervisors for their feedback during my writing of this thesis.

Morten Rieger Hannemose, [Assistant Professor], [affiliation]

[text]

[Name], [Title], [affiliation]

[text]

Contents

Preface	ii
Abstract	iii
Acknowledgements	iv
1 Introduction	1
2 Background	3
2.1 Skinned Multi-Person Linear Model (SMPL)	3
2.2 Human Mesh Reconstruction (HMR)	3
2.3 Denoising Diffusion Probabilistic Models (DDPM)	4
2.3.1 Variance schedules	6
2.3.2 Classifier and Classifier-Free Guidance (CFG)	6
2.4 Transformer architecture	7
2.5 Human Motion Generation	9
3 Data	11
3.1 HumanML3D	11
3.2 InterHuman	11
3.3 Teton dataset	11
4 Methods	13
4.1 Tracking & Matching	13
4.2 Human pose sequence optimization	13
4.3 3D scene reconstruction	13
4.4 Aligning datasets	14
4.5 Motion and scene representation	14
4.6 Diffusion model	15
5 Results	17
6 Discussion & Conclusion	19
Bibliography	21
A Appendices	23
A.1 Derivation of posterior distribution	23
A.2 L_{t-1} closed form derivation	23

1 Introduction

In healthcare environments such as hospitals and care homes, data pertaining to critical incidents like falls are scarce due to their infrequent nature and the high privacy requirements surrounding such data. This scarcity poses significant challenges for training robust machine learning models, particularly in applications related to video classification where detailed understanding of such events is crucial. The primary goal of this thesis is to enhance the performance of video classification tasks by leveraging synthetic data, which is designed to closely mirror the underlying distribution of real-world incidents while enabling focused studies on specific, rare events.

To address the challenges inherent in collecting and utilizing real-world data from sensitive environments, this research proposes a novel approach using synthetic data generation. Synthetic data not only adheres to the distributional characteristics of genuine data but also provides flexibility to explore less common scenarios—specifically, those at the tail of the distribution which are typically underrepresented in available datasets.

This work introduces a sophisticated framework for generating synthetic data by explicitly modeling three-dimensional (3D) environments. This includes detailed interactions both among humans and between humans and their surroundings. By integrating these complex interactions as a strong inductive bias, the proposed generative diffusion model enhances the realism and applicability of the synthetic data.

To construct and train this model, we utilize publicly available datasets such as HumanML3D and InterHuman. These datasets include motion capture data of individuals and pairs interacting, each accompanied by textual descriptions. These are combined with 3D scene reconstructions derived from video captures in actual hospital and care home settings. This integration of human motion and scene specifics forms the foundation for our synthetic data generation process.

To effectively reconstruct 3D scenes from the captured videos, we employ state-of-the-art models such as ProHMR and Depth Anything. These models are instrumental in generating per-frame human pose estimations and scene depth labels. These outputs, along with 2D keypoint annotations, are fed into a joint optimization process. This process is critical as it unifies the coordinate systems of the human models and the environment, ensuring that the motion trajectories are smooth and coherent. The result is a highly accurate 3D representation of the scenes, which serves as a vital input for our synthetic data generation.

2 Background

2.1 Skinned Multi-Person Linear Model (SMPL)

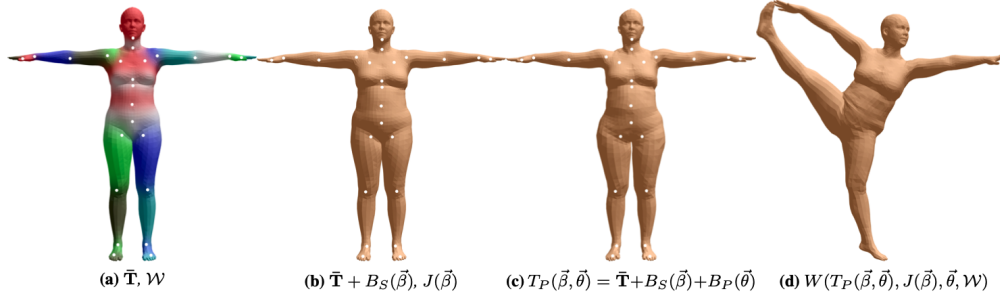


Figure 2.1: SMPL model

The Skinned Multi-Person Linear (SMPL) model is a parametric body shape model that accurately represents a wide range of human bodies and poses. It is built upon a foundation of linear blend skinning enhanced with corrective blend shapes, which are derived from a large dataset of body scans. The model captures the subtle deformations that occur with different body shapes and poses and can easily be rendered due to its compatibility with existing graphics pipelines. Since its publication, several extensions such as DMPL, incorporating dynamic soft-tissue deformation and SMPL-X, also modelling hands and facial expressions have been introduced. The model is parameterized by $\vec{\beta}$, capturing the variations from a mean body shape and $\vec{\theta}$, specifying the axis-angle rotation of 23 of the template skeleton joints. Mathematically, the model can be expressed as:

$$M(\vec{\beta}, \vec{\theta}) = W(T_P(\vec{\beta}, \vec{\theta}), J(\vec{\beta}), \vec{\theta}, \mathcal{W}) \quad (2.1)$$

where $T_P(\vec{\beta}, \vec{\theta})$ returns the vertices of the rest pose, incorporating the deformations from the body shape and pose and is given by:

$$T_P(\vec{\beta}, \vec{\theta}) = \bar{\mathbf{T}} + B_S(\vec{\beta}) + B_P(\vec{\theta}) \quad (2.2)$$

$J(\vec{\beta})$ returns the 3D joint locations from the shaped template vertices using a learned regression matrix \mathcal{J} and is given by:

$$J(\vec{\beta}) = \mathcal{J}(\bar{\mathbf{T}} + B_S(\vec{\beta})) \quad (2.3)$$

W is the skinning function (e.g. Linear Blend Skinning (LBS) or Dual-Quaternion Blend Skinning (DQBS)) and \mathcal{W} is the blend weights.

2.2 Human Mesh Reconstruction (HMR)

Recovering the mesh of humans have several applications...

2.3 Denoising Diffusion Probabilistic Models (DDPM)

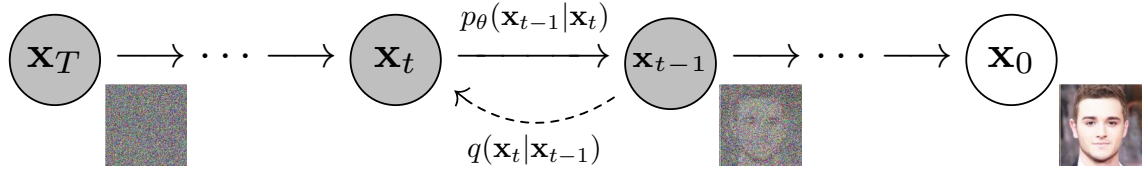


Figure 2.2: Diffusion forward and backward process (taken from Ho, Jain, and Abbeel 2020)

In recent years, several types of generative models such as Variational Autoencoders (VAEs), Generative Adversarial Networks (GANs), autoregressive models and flow-based models have shown remarkable results in data generation of varying data modalities, such as images, audio, videos and text. Most recently, Denoising Diffusion Probabilistic Models (DDPMs) have gained large popularity especially within the field of image generation due to several reasons such as high-quality data generation, versatility in several data domains as well as controllability, allowing one to steer the generation towards desired outputs.

A DDPM is a parametrized Markov chain trained using variational inference to reverse a (forward) diffusion process, $q(\mathbf{x}_{1:T} \mid \mathbf{x}_0)$, as seen in fig. 2.2 wherein the signal of the data, \mathbf{x}_0 , is gradually destroyed by adding gaussian noise according to predefined noise schedule $\{\beta_t \in (0, 1)\}_{t=1}^T$ giving rise to increasingly noisy samples, $\mathbf{x}_1 \dots \mathbf{x}_T$.

The forward process is defined as follows:

$$q(\mathbf{x}_{1:T} \mid \mathbf{x}_0) = \prod_{t=1}^T q(\mathbf{x}_t \mid \mathbf{x}_{t-1}), \quad q(\mathbf{x}_t \mid \mathbf{x}_{t-1}) = \mathcal{N}(x_t; \sqrt{1 - \beta_t} \mathbf{x}_t, \beta_t \mathbf{I}) \quad (2.4)$$

with T being the discretized number of diffusion steps before all original information is completely discarded. The goal of the inverse or backwards process then becomes to iteratively remove the noise, in order to arrive at the original data. More formally, the process is defined as:

$$p_\theta(\mathbf{x}_{0:T}) = p(\mathbf{x}_T) \prod_{t=1}^T p_\theta(\mathbf{x}_{t-1} \mid \mathbf{x}_t), \quad p_\theta(\mathbf{x}_{t-1} \mid \mathbf{x}_t) = \mathcal{N}(\mathbf{x}_{t-1}; \boldsymbol{\mu}_\theta(\mathbf{x}_t, t), \boldsymbol{\Sigma}_\theta(\mathbf{x}_t, t)) \quad (2.5)$$

taking starting point in pure noise $p(\mathbf{x}_T) = \mathcal{N}(\mathbf{x}_T; \mathbf{0}, \mathbf{I})$, incrementally removing the noise through the learned functions, $\boldsymbol{\mu}_\theta(\mathbf{x}_t, t)$ and $\boldsymbol{\Sigma}_\theta(\mathbf{x}_t, t)$ commonly parameterized by a deep neural network. Using the reparameterization trick, we are able to sample any noisy version of our data, \mathbf{x}_t , at time step t given our original data \mathbf{x}_0 . Recall our forward transition probability function, $q(\mathbf{x}_t \mid \mathbf{x}_{t-1})$. Letting $\alpha_t = 1 - \beta_t$, $\bar{\alpha}_t = \prod_{i=1}^t \alpha_i$ and using the reparameterization trick the expression can be rewritten as:

$$\mathbf{x}_t = \sqrt{\alpha_t} \mathbf{x}_{t-1} + \sqrt{1 - \alpha_t} \epsilon_{t-1} \quad (2.6)$$

where $\epsilon_{t-1} \sim \mathcal{N}(0, 1)$. Expanding the recursive definition then gives:

$$\begin{aligned} \mathbf{x}_t &= \sqrt{\alpha_t} \left(\sqrt{\alpha_{t-1}} \mathbf{x}_{t-2} + \sqrt{1 - \alpha_{t-1}} \epsilon_{t-2} \right) + \sqrt{1 - \alpha_t} \epsilon_{t-1} \\ &= \sqrt{\alpha_t \alpha_{t-1}} \mathbf{x}_{t-2} + \sqrt{1 - \alpha_t \alpha_{t-1}} \bar{\epsilon}_{t-2} \end{aligned}$$

where $\bar{\epsilon}_{t-2}$ merges the two independent Gaussians ϵ_{t-1} and ϵ_{t-2} into a single Gaussian with new variance as the sum of variances $\alpha_t(1 - \alpha_{t-1}) + (1 - \alpha_t) = 1 - \alpha_t \alpha_{t-1}$. Recursively

applying the definition of \mathbf{x}_t and merging the gaussian noise terms results in the simplified expression:

$$\mathbf{x}_t = \sqrt{\bar{\alpha}_t} \mathbf{x}_0 + \sqrt{1 - \bar{\alpha}_t} \boldsymbol{\epsilon}, \quad \boldsymbol{\epsilon} \sim \mathcal{N}(\mathbf{0}, \mathbf{I}) \quad (2.7)$$

Conversely, given \mathbf{x}_0 , the reverse conditional probability:

$$q(\mathbf{x}_{t-1} | \mathbf{x}_t, \mathbf{x}_0) = \mathcal{N}\left(\mathbf{x}_{t-1}; \tilde{\boldsymbol{\mu}}_t(\mathbf{x}_t, \mathbf{x}_0), \tilde{\beta}_t \mathbf{I}\right)$$

becomes tractable to compute using Bayes rule (derivation in appendix A.1) with mean and variance given by:

$$\tilde{\boldsymbol{\mu}}_t(\mathbf{x}_t, \mathbf{x}_0) = \frac{\sqrt{\bar{\alpha}_{t-1}} \beta_t}{1 - \bar{\alpha}_t} \mathbf{x}_0 + \frac{\sqrt{\bar{\alpha}_t} (1 - \bar{\alpha}_{t-1})}{1 - \bar{\alpha}_t} \mathbf{x}_t \stackrel{\text{Using 2.7}}{=} \frac{1}{\sqrt{\bar{\alpha}_t}} \left(\mathbf{x}_t - \frac{1 - \alpha_t}{\sqrt{1 - \bar{\alpha}_t}} \boldsymbol{\epsilon}_t \right) \quad (2.8)$$

$$\tilde{\beta}_t = \frac{1 - \bar{\alpha}_{t-1}}{1 - \bar{\alpha}_t} \beta_t \quad (2.9)$$

The model is trained by optimizing the variational lower bound on the log likelihood:

$$L_{VLB} = \mathbb{E}_q \left[\log \frac{p_\theta(\mathbf{x}_{0:T})}{q(\mathbf{x}_{1:T} | \mathbf{x}_0)} \right] = \mathbb{E}_q \left[\log p(\mathbf{x}_T) + \sum_{t \geq 1} \log \frac{p_\theta(\mathbf{x}_{t-1} | \mathbf{x}_t)}{q(\mathbf{x}_t | \mathbf{x}_{t-1})} \right] \leq \mathbb{E} [\log p_\theta(\mathbf{x}_0)] \quad (2.10)$$

which in practice means minimizing the negative variational lower bound. Ho, Jain, and Abbeel 2020 rewrites this into a sum of KL-divergences:

$$L_{VLB} = \mathbb{E}_q \left[\underbrace{D_{KL}(q(\mathbf{x}_T | \mathbf{x}_0) \| p(\mathbf{x}_T))}_{L_T} + \sum_{t=2}^T \underbrace{D_{KL}(q(\mathbf{x}_{t-1} | \mathbf{x}_t, \mathbf{x}_0) \| p_\theta(\mathbf{x}_{t-1} | \mathbf{x}_t))}_{L_{t-1}} - \underbrace{\log p_\theta(\mathbf{x}_0 | \mathbf{x}_1)}_{L_0} \right] \quad (2.11)$$

where the authors model L_0 from separate discrete decoder. As L_T doesn't depend on our parameters, θ , and is therefore constant, it can be ignored during optimization. The rest of the L_{t-1} terms can be efficiently computed in the closed form, by fixing the variance $\Sigma_\theta(\mathbf{x}_t, t) = \sigma_t^2 \mathbf{I}$ to only depend on the current timestep (authors propose $\sigma_t^2 = \beta_t$ or $\sigma_t^2 = \tilde{\beta}_t$). L_{t-1} can then be written in closed form (derivation in appendix A.2) as:

$$L_{t-1} = \mathbb{E}_q \left[\frac{1}{2\sigma_t^2} \|\tilde{\boldsymbol{\mu}}_t(\mathbf{x}_t, \mathbf{x}_0) - \boldsymbol{\mu}_\theta(\mathbf{x}_t, t)\|^2 \right] + C_t \quad (2.12)$$

where C_t is a constant depending on the choice of σ_t^2 and the noise schedule. Using eq. (2.8) Ho, Jain, and Abbeel 2020 reparameterize the expression in terms of predicting the noise:

$$L_{t-1} = \mathbb{E}_{\mathbf{x}_0, \boldsymbol{\epsilon}} \left[\frac{\beta_t^2}{2\sigma_t^2 \alpha_t (1 - \bar{\alpha}_t)} \|\boldsymbol{\epsilon} - \boldsymbol{\epsilon}_\theta(\sqrt{\bar{\alpha}_t} \mathbf{x}_0 + \sqrt{1 - \bar{\alpha}_t} \boldsymbol{\epsilon}, t)\|^2 \right] \quad (2.13)$$

as they find it leads to better unconditional sample quality when training on the CIFAR10 dataset. Furthermore, they report the best sample quality when using the "simple" objective, ignoring the weighing:

$$L_{\text{simple}} = \mathbb{E}_{t \sim \mathcal{U}(1, T), \boldsymbol{\epsilon}} [\boldsymbol{\epsilon} - \boldsymbol{\epsilon}_\theta(\sqrt{\bar{\alpha}} \mathbf{x}_0 + \sqrt{1 - \bar{\alpha}} \boldsymbol{\epsilon}, t)] \quad (2.14)$$

The final training and sampling scheme, as outlined in algorithm 1 and algorithm 2 can be summarized as follows. The training algorithm optimizes the model to predict and remove noise from data, while the sampling algorithm uses the trained model to iteratively transform random noise into structured data.

Algorithm 1 Training

```

1: repeat
2:    $\mathbf{x}_0 \sim q(\mathbf{x}_0)$ 
3:    $t \sim \text{Uniform}(\{1, \dots, T\})$ 
4:    $\epsilon \sim \mathcal{N}(\mathbf{0}, \mathbf{I})$ 
5:   Take gradient descent step on
       $\nabla_{\theta} \|\epsilon - \epsilon_{\theta}(\sqrt{\bar{\alpha}_t} \mathbf{x}_0 + \sqrt{1 - \bar{\alpha}_t} \epsilon, t)\|^2$ 
6: until converged

```

Algorithm 2 Sampling

```

1:  $\mathbf{x}_T \sim \mathcal{N}(\mathbf{0}, \mathbf{I})$ 
2: for  $t = T, \dots, 1$  do
3:    $\mathbf{z} \sim \mathcal{N}(\mathbf{0}, \mathbf{I})$  if  $t > 1$ , else  $\mathbf{z} = \mathbf{0}$ 
4:    $\mathbf{x}_{t-1} = \frac{1}{\sqrt{\bar{\alpha}_t}} \left( \mathbf{x}_t - \frac{1 - \bar{\alpha}_t}{\sqrt{1 - \bar{\alpha}_t}} \epsilon_{\theta}(\mathbf{x}_t, t) \right) + \sigma_t \mathbf{z}$ 
5: end for
6: return  $\mathbf{x}_0$ 

```

2.3.1 Variance schedules

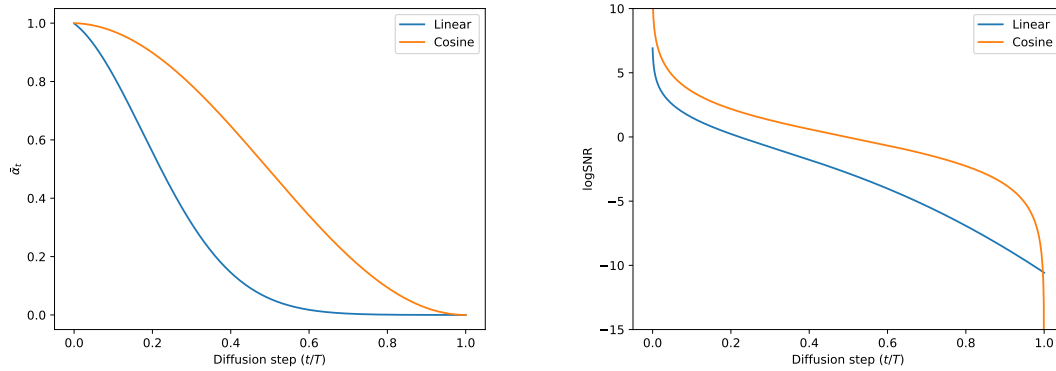


Figure 2.3: Linear and cosine schedule and signal-to-noise ratio.

In the DDPM paper Ho, Jain, and Abbeel 2020 choose a variance schedule with β_t linearly increasing from $\beta_1 = 10^{-4}$ to $\beta_T = 0.02$. However, this results in \mathbf{x}_t almost entirely losing its signal in the last quarter of the schedule as problematized by A. Q. Nichol and Dhariwal 2021. The authors instead propose a cosine variance schedule, where the squared signal proportion is given by:

$$\bar{\alpha}_t = \frac{f(t)}{f(0)}, \quad f(t) = \cos \left(\frac{t/T + s}{1+s} \cdot \frac{\pi}{2} \right)^2 \quad (2.15)$$

where s controls the offset of the noise schedule. The authors set $s = 0.008$ as they found that $s = 0$ resulted in minuscule noise near $t = 0$ making it hard for the model to predict ϵ . From $\bar{\alpha}_t$ one can then compute $\beta_t = \min \left(1 - \frac{\bar{\alpha}_t}{\bar{\alpha}_{t-1}}, 0.999 \right)$ with the min to prevent singularities. A comparison of the cosine and linear schedules can be seen in fig. 2.3.

2.3.2 Classifier and Classifier-Free Guidance (CFG)

In practice, it is often desirable to steer the generation process in order to output data belonging to a specific class, such as cats or dogs in the context of image generation, or incorporating some other information relevant for the output. This process can be framed within the context of probability theory as conditional generation, where the aim is to maximize the probability of the data, \mathbf{x} , given some conditioning signal, y , (e.g. a class label). According to Bayes' rule, the conditional probability can be expressed as:

$$p(\mathbf{x} | y) = \frac{p(\mathbf{x}, y)}{p(y)} \propto p(y | \mathbf{x})p(\mathbf{x}) \quad (2.16)$$

Hence, it is proportional to the joint probability of the data and label, which from basic probability theory is equal to the product of the unconditional probability of the data, $p(\mathbf{x})$,

and the probability of the conditioning signal given the data, $p(y | \mathbf{x})$ (for labels; that the data belonging to the given class). In the DDPM paper Ho, Jain, and Abbeel 2020 establishes connection between diffusion models and Noise-Conditioned Score Networks (NCSN) and shows how the reverse diffusion process can be seen as a temporal discretized type of annealed Langevin dynamics given by the stochastic differential equation:

$$\frac{d}{dt} \log p(\mathbf{x}_t) = \sqrt{\bar{\alpha}_t} s(\mathbf{x}_t, t) + \sqrt{1 - \bar{\alpha}_t} \mathbf{z}_t \quad (2.17)$$

where $\mathbf{z}_t \sim \mathcal{N}(0, 1)$ and $s(\mathbf{x}_t, t) = \nabla_{\mathbf{x}_t} \log p(\mathbf{x}_t)$ is referred to as the score function. It turns out that the denoising network can be used to approximate the score function:

$$s(\mathbf{x}_t, t) \approx -\frac{1}{\sqrt{1 - \bar{\alpha}_t}} \epsilon_\theta(\mathbf{x}_t, t) \quad (2.18)$$

Returning to the factorization of the conditional probability, taking the gradient of the log of both sides reveals the relationship with the score function:

$$\nabla_{\mathbf{x}_t} \log p(\mathbf{x}_t | y) = \nabla_{\mathbf{x}_t} \log p(y | \mathbf{x}_t) + \underbrace{\nabla_{\mathbf{x}_t} \log p(\mathbf{x}_t)}_{s(\mathbf{x}_t, t)} \quad (2.19)$$

Dhariwal and A. Nichol 2021 trains a classifier, $f_\phi(y | \mathbf{x}_t) \approx p(y | \mathbf{x}_t)$, separately to predict the class label of noisy images. By using the reformulated denoising function:

$$\bar{\epsilon}_\theta(\mathbf{x}_t, t) = \epsilon_\theta(\mathbf{x}_t, t) - \sqrt{1 - \bar{\alpha}_t} \nabla_{\mathbf{x}_t} \log f_\phi(y | \mathbf{x}_t) \quad (2.20)$$

where s controls guidance strength, it is possible to guide the diffusion sampling e.g. in order to generate images of a specific category, hence the name classifier guidance.

2.4 Transformer architecture

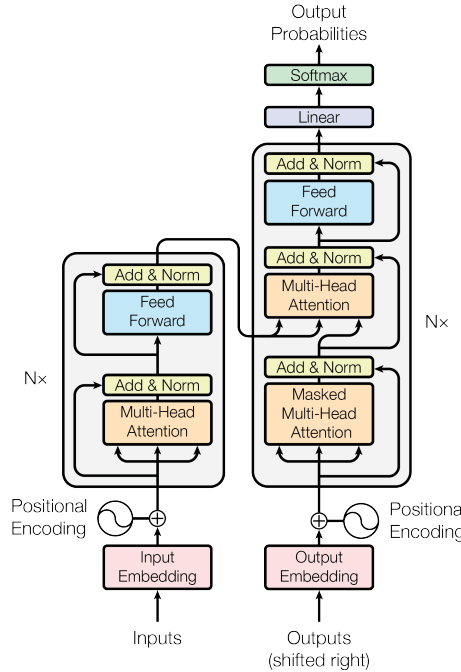


Figure 2.4: The transformer (Image from Vaswani et al. 2017.)

The transformer model, introduced by Vaswani et al. 2017, revolutionized natural language processing (NLP) and machine translation. This model was designed as an alternative to the traditional recurrent sequence models, such as the seq2seq model by Sutskever, Vinyals, and Le 2014, which had been widely used in NLP tasks.

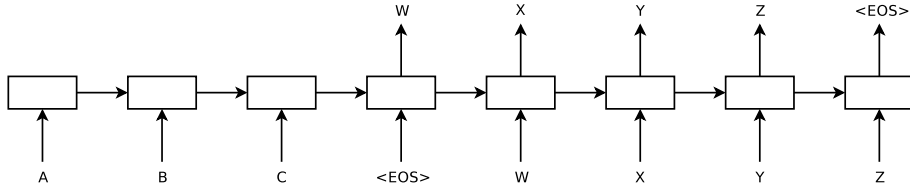


Figure 2.5: The seq2seq model by Sutskever, Vinyals, and Le 2014.

The seq2seq model (as illustrated in fig. 2.5) encodes an input sequence into a context vector and then decodes the output sequence from this vector in a sequential manner. This approach often results in an information bottleneck, particularly when dealing with long-range dependencies within the data.

In contrast, the transformer model utilizes an attention mechanism, enabling more effective communication between tokens without relying on sequential processing of hidden states. The architecture comprises an encoder and a decoder. The encoder uses multi-headed self-attention to create semantic representations for each token in the input sequence, allowing the model to process the entire context simultaneously.

The decoder then uses these representations through cross-attention and causal self-attention mechanisms. Cross-attention integrates information from the encoder's output, while causal self-attention ensures that the model only considers previously generated tokens by masking out future tokens in the training phase. At inference time, the output tokens are generated autoregressively.

One of the key strengths of the transformer model is its training efficiency, owing to the parallelizable nature of the attention mechanism. During the generation process, tokens are produced in an autoregressive fashion, with each generated token serving as context for the subsequent one.

The transformer's attention mechanism is based on scaled dot-product attention, defined by the following equation:

$$\text{Attention}(Q, K, V) = \text{softmax} \left(\frac{QK^T}{\sqrt{d_k}} \right) V \quad (2.21)$$

Q , K and V are the query, key, and value matrices, respectively, and d_k is the dimension of the key vectors.

For causal self-attention, the model masks future tokens for each key to prevent information leakage, ensuring the model attends only to past and present tokens during both training and inference.

Since the transformer architecture does not inherently encode positional information, Vaswani et al. introduced a sinusoidal positional encoding scheme. This scheme incorporates positional information into each element of the input sequence, defined as:

2.5 Human Motion Generation

Generating realistic human motion has several applications

- Human Motion Diffusion -

3 Data

3.1 HumanML3D

The HumanML3D dataset combines the HumanAct12 and AMASS datasets, integrating human motion captured using advanced motion capturing systems and converting the data to a unified parameterization. It covers a broad range of daily human activities, providing 14,616 motions in total, accompanied by 44,970 single-sentence descriptions. Each motion clip includes 3-4 descriptions, and the entire dataset amounts to 28.59 hours of recorded motion. Additionally, the data is augmented by mirroring all motions, with corresponding adjustments to descriptions, such as changing “clockwise” to “counterclockwise.”

3.2 InterHuman

The InterHuman dataset is a comprehensive, large-scale 3D dataset designed to capture human interactive motions involving two individuals. It includes approximately 107 million frames detailing a wide range of human interactions, from professional activities to daily social behaviors. Each motion sequence is paired with natural language annotations, totaling 23,337 descriptions, which provide context and detail for the captured interactions, enhancing the dataset’s utility for training and evaluating models.

3.3 Teton dataset



Figure 3.1: Examples from the Teton dataset

The Teton dataset contains approximately 50,000 image sequences hierarchically organized by hospital/carehome site, room and timestamp. Each sequence consists of 100 frames recorded at approximately 10 frames per second, resulting in a sequence duration of about 10 seconds and totaling roughly 140 hours of data.

Each person in the frame has been manually annotated with their class (person, staff, patient), center point, bounding box, keypoints and current action (e.g., “laying in bed”, “standing on floor”). Using an image similarity threshold, the 100 frames are reduced to

a smaller set of key frames. Each key frame is annotated with segmentation masks for people in the frame as well as the floor, walls and furniture (e.g., beds, sofas and chairs).

As the dataset is inherently two dimensional and does not contain 3D annotations such as poses or depth maps, we instead rely on pseudo-ground truth data derived from off-the-shelf models. In the case of human poses the HMR2.0 model by Goel et al. 2023 is initially run on the image sequences to predict a set of poses. Poses with high reprojection error are filtered out, and the remaining poses with low reprojection error are used as pseudo-ground truth.

For reconstructing depth maps the monocular metric depth estimation model, Depth Anything by Yang et al. 2024, trained on the indoor NYUv2 dataset (Nathan Silberman and Fergus 2012), is applied to the set of key frames.

4 Methods

4.1 Tracking & Matching

We track the predicted staff and patients across multiple frames, indicated by $t = 1 \dots T$, by iteratively assigning the predictions, $\{P_i^{(t)}\}_{i=1}^{M_t}$, to the latest known tracks, $\{Q_j^{(t)}\}_{j=1}^{N_t}$ by greedily picking the assignment with the minimum cost:

$$\underset{i,j}{\operatorname{argmin}} \mathcal{L}_{\text{track}}(P_i^{(t)}, Q_j^{(t-1)}), \quad (4.1)$$

until either all predictions or latest tracks have been assigned exactly once. In the case of any unassigned predictions, a new track is initialized. After tracks have been assigned, the latest track $Q_j^{(t)}$ is updated with the assigned predictions. We choose the following composite loss function:

$$\mathcal{L}_{\text{track}}(P, Q) = \alpha \|P_{\text{3D kpts}} - Q_{\text{3D kpts}}\|_2 + \beta \|P_{\text{class}} - Q_{\text{class}}\|_\infty, \quad (4.2)$$

incorporating both the Euclidean distance between the 3D joint keypoints as well as the predicted person class (staff/patient), with α and β weighting the influence of each term. The tracks, T_i , are then greedily matched to the ground truth annotations G_j , minimizing the loss:

$$\mathcal{L}_{\text{match}}(T, G) = \sum_t^T \begin{cases} \left\| a_{\text{track}, \text{2D kpts}}^{(t)} - b_{\text{track}, \text{2D kpts}}^{(t)} \right\|_2 & \text{if } a_{\text{track}}^{(t)} \in a_{\text{track}} \\ \gamma & \text{otherwise} \end{cases} \quad (4.3)$$

over the trajectory time horizon $t = 1, 2, \dots, T$ where γ is the punishment for not detecting the person.

4.2 Human pose sequence optimization

4.3 3D scene reconstruction

Restoring depth scale and offsets

We utilize pseudo ground truth disparity maps generated by the Depth Anything model, inversely proportional to the scene depth, in order to reconstruct a point cloud of the scene. To recover the depth scale and offset we rasterize the predicted SMPL poses, extract the z-buffer, compute the inverse depth and regress the intersection with the normalized disparity maps using the Random Sample Consensus (RANSAC) algorithm robust to outliers.

$$\begin{bmatrix} px \\ y \\ 1/z \\ 1 \end{bmatrix} = \begin{bmatrix} f_x & 0 & 0 & p_x \\ 0 & f_y & 0 & p_y \\ 0 & 0 & 1 & 0 \\ 0 & 0 & 0 & 1 \end{bmatrix} \begin{bmatrix} X \\ Y \\ Z \\ 1 \end{bmatrix} \quad (4.4)$$

$$X = \frac{Z}{f_x} (x - p_x), \quad Y = \frac{Z}{f_x} (y - p_y) \quad (4.5)$$

where f_x , f_y are the horizontal and vertical focal lengths respectively and (p_x, p_y) is the principal point often chosen as the center $(w/2, h/2)$ of the image.

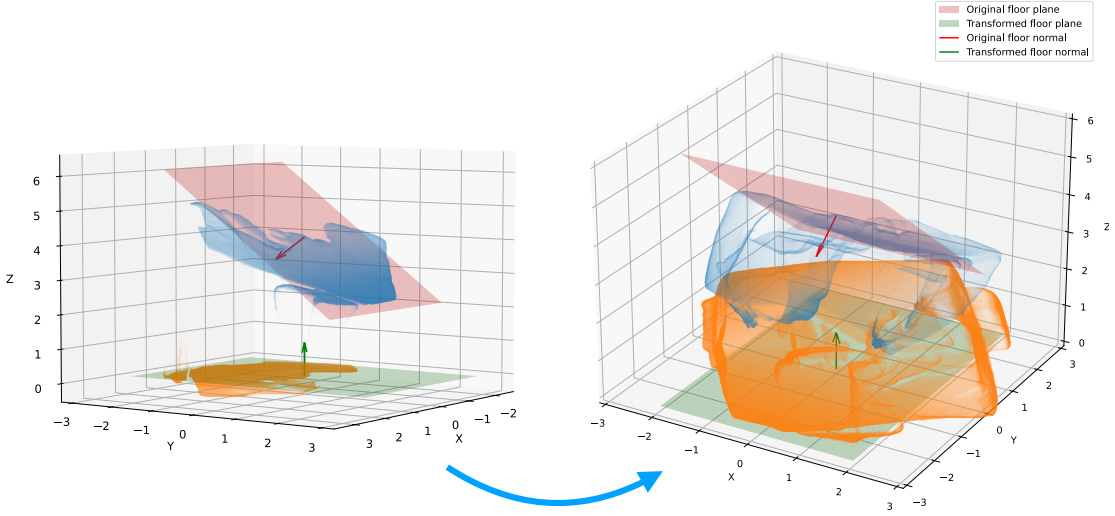


Figure 4.1: Translation and rotation of room point cloud to align floor with XY-plane.

4.4 Aligning datasets

To compute the rotation matrix that aligns the normal vector $\hat{\mathbf{n}}_{\text{floor}} = \mathbf{n}_{\text{floor}} / \|\mathbf{n}_{\text{floor}}\|$ (where $\mathbf{n}_{\text{floor}} = (0, 1, \mathbf{b}_1)^T \times (1, 0, \mathbf{b}_0)^T$) of the floor plan in the camera coordinate system with the normal vector $\mathbf{n}_{xy} = (0, 0, 1)$ of the xy-plane, we can utilize Rodrigues' rotation formula.

First, we construct the skew-symmetric matrix \mathbf{K} from the components of the cross product vector $\mathbf{v} = \hat{\mathbf{n}}_{\text{floor}} \times \mathbf{n}_{xy}$. The skew-symmetric matrix \mathbf{K} is defined as:

$$\mathbf{K} = \begin{bmatrix} 0 & -v_3 & v_2 \\ v_3 & 0 & -v_1 \\ -v_2 & v_1 & 0 \end{bmatrix} \quad (4.6)$$

Next, we compute the rotation matrix \mathbf{R} using Rodrigues' rotation formula. The formula incorporates the identity matrix \mathbf{I} , the skew-symmetric matrix \mathbf{K} , and a scaling term based on the angle between the vectors. The resulting rotation matrix is given by:

$$\mathbf{R} = \mathbf{I} + \mathbf{K} + \mathbf{K}^2 \left(\frac{1 - c}{s^2} \right) \quad (4.7)$$

Here, \mathbf{I} is the identity matrix, c is the dot product of \mathbf{a} and \mathbf{b} , and s is the norm of the cross product vector \mathbf{v} . This formula ensures that the rotation matrix \mathbf{R} not only aligns \mathbf{a} with \mathbf{b} but also preserves the orthogonality and orientation of the coordinate system.

Finally, we transform the point cloud by translating it to align the floor plane intercept with the origin, followed by rotating it using the computed rotation matrix:

$$\mathbf{p}^* = \mathbf{R} (\mathbf{p} - (0, 0, b_0)^T) \quad (4.8)$$

4.5 Motion and scene representation

Previous work on single human motion generation uses a canonical representation

We use a 6D continuous representation of the joint angles as according to Zhou et al. 2019.

4.6 Diffusion model

5 Results

6 Discussion & Conclusion

Bibliography

- Ho, Jonathan, Ajay Jain, and Pieter Abbeel (2020). “Denoising diffusion probabilistic models”. In: *Advances in neural information processing systems* 33, pp. 6840–6851.
- Nichol, Alexander Quinn and Prafulla Dhariwal (18–24 Jul 2021). “Improved Denoising Diffusion Probabilistic Models”. In: *Proceedings of the 38th International Conference on Machine Learning*. Ed. by Marina Meila and Tong Zhang. Vol. 139. Proceedings of Machine Learning Research. PMLR, pp. 8162–8171. URL: <https://proceedings.mlr.press/v139/nichol21a.html>.
- Dhariwal, Prafulla and Alexander Nichol (2021). “Diffusion Models Beat GANs on Image Synthesis”. In: *Advances in Neural Information Processing Systems*. Ed. by M. Ranzato et al. Vol. 34. Curran Associates, Inc., pp. 8780–8794. URL: https://proceedings.neurips.cc/paper_files/paper/2021/file/49ad23d1ec9fa4bd8d77d02681df5cfa-Paper.pdf.
- Vaswani, Ashish et al. (2017). “Attention is All you Need”. In: *Advances in Neural Information Processing Systems*. Ed. by I. Guyon et al. Vol. 30. Curran Associates, Inc. URL: https://proceedings.neurips.cc/paper_files/paper/2017/file/3f5ee243547dee91fdb053c1c4a845aa-Paper.pdf.
- Sutskever, Ilya, Oriol Vinyals, and Quoc V. Le (2014). “Sequence to sequence learning with neural networks”. In: *Proceedings of the 27th International Conference on Neural Information Processing Systems - Volume 2*. NIPS’14. Montreal, Canada: MIT Press, pp. 3104–3112.
- Goel, Shubham et al. (2023). “Humans in 4D: Reconstructing and Tracking Humans with Transformers”. In: *International Conference on Computer Vision (ICCV)*.
- Yang, Lihe et al. (2024). “Depth Anything: Unleashing the Power of Large-Scale Unlabeled Data”. In: *CVPR*.
- Nathan Silberman Derek Hoiem, Pushmeet Kohli and Rob Fergus (2012). “Indoor Segmentation and Support Inference from RGBD Images”. In: *ECCV*.
- Zhou, Yi et al. (June 2019). “On the Continuity of Rotation Representations in Neural Networks”. In: *The IEEE Conference on Computer Vision and Pattern Recognition (CVPR)*.

A Appendices

A.1 Derivation of posterior distribution

$$\begin{aligned}
q(\mathbf{x}_{t-1} | \mathbf{x}_t, \mathbf{x}_0) &= q(\mathbf{x}_t | \mathbf{x}_{t-1}, \mathbf{x}_0) \frac{q(\mathbf{x}_{t-1} | \mathbf{x}_0)}{q(\mathbf{x}_t | \mathbf{x}_0)} \\
\Leftrightarrow \log q(\mathbf{x}_{t-1} | \mathbf{x}_t, \mathbf{x}_0) &= \log q(\mathbf{x}_t | \mathbf{x}_{t-1}, \mathbf{x}_0) + \log q(\mathbf{x}_{t-1} | \mathbf{x}_0) - \log q(\mathbf{x}_t | \mathbf{x}_0) \\
&= \frac{1}{2} \left(\frac{(\mathbf{x}_t - \sqrt{\alpha_t} \mathbf{x}_{t-1})^2}{\beta_t} + \frac{(\mathbf{x}_{t-1} - \sqrt{\bar{\alpha}_{t-1}} \mathbf{x}_0)^2}{1 - \bar{\alpha}_{t-1}} + \frac{(\mathbf{x}_t - \sqrt{\bar{\alpha}_t} \mathbf{x}_0)^2}{1 - \bar{\alpha}_t} \right) + K \\
&= \frac{1}{2} \left(\frac{\mathbf{x}_t^2 - 2\sqrt{\alpha_t} \mathbf{x}_t \mathbf{x}_{t-1} + \alpha_t \mathbf{x}_{t-1}^2}{\beta_t} + \frac{\mathbf{x}_{t-1}^2 - 2\sqrt{\bar{\alpha}_{t-1}} \mathbf{x}_{t-1} \mathbf{x}_0 + \bar{\alpha}_{t-1} \mathbf{x}_0^2}{1 - \bar{\alpha}_{t-1}} + C(x_t, x_0) \right) +
\end{aligned}$$

We collect all terms for \mathbf{x}_{t-1} and \mathbf{x}_{t-1}^2 .

A.2 L_{t-1} closed form derivation

The closed form of the KL-divergence between two Gaussians $\mathcal{N}_0(\mu_0, \Sigma_0)$, $\mathcal{N}_1(\mu_1, \Sigma_1)$ is given as:

$$D_{\text{KL}}(\mathcal{N}_0 \| \mathcal{N}_1) = \frac{1}{2} \left(\text{tr}(\Sigma_1^{-1} \Sigma_0) - k + (\mu_1 - \mu_0)^T \Sigma_1^{-1} (\mu_1 - \mu_0) + \ln \frac{\det \Sigma_1}{\det \Sigma_0} \right) \quad (\text{A.1})$$

Inserting $q(\mathbf{x}_{t-1} | \mathbf{x}_t, \mathbf{x}_0) = \mathcal{N}(\mathbf{x}_{t-1}; \tilde{\mu}_t(\mathbf{x}_t, \mathbf{x}_0), \tilde{\beta}_t \mathbf{I})$ and $p(\mathbf{x}_t | \mathbf{x}_{t-1}) = \mathcal{N}(\mathbf{x}_t; \mu_\theta(\mathbf{x}_t, t), \sigma_t^2 \mathbf{I})$ yields:

$$D_{\text{KL}}(q \| p) = \frac{1}{2} \left(k \frac{\tilde{\beta}_t}{\sigma_t^2} - k + \frac{1}{\sigma_t^2} \|\tilde{\mu}_t(\mathbf{x}_t, \mathbf{x}_0) - \mu_\theta(\mathbf{x}_t, t)\|^2 + \ln(\sigma_t^2) - \ln(\tilde{\beta}_t) \right) \quad (\text{A.2})$$

Letting $\sigma_t^2 = \tilde{\beta}_t$ ($= \beta_t = \frac{1-\bar{\alpha}_t}{1-\bar{\alpha}_{t-1}} \tilde{\beta}_t$) simplifies the above to:

$$D_{\text{KL}}(q \| p) = \frac{1}{2\sigma_t^2} \|\tilde{\mu}_t(\mathbf{x}_t, \mathbf{x}_0) - \mu_\theta(\mathbf{x}_t, t)\|^2 (+ C_t) \quad (\text{A.3})$$

where C_t is a constant depending only on the noise schedule.

Hello, here is some text without a meaning. This text should show what a printed text will look like at this place. If you read this text, you will get no information. Really? Is there no information? Is there a difference between this text and some nonsense like "Huardest gefburn"? Kjift – not at all! A blind text like this gives you information about the selected font, how the letters are written and an impression of the look. This text should contain all letters of the alphabet and it should be written in of the original language. There is no need for special content, but the length of words should match the language.

Technical
University of
Denmark

Richard Petersens Plads, Building 324
2800 Kgs. Lyngby
Tlf. 4525 1700

www.compute.dtu.dk